Molecular Therapy
Methods & Clinical Development
Original Article

Biolayer interferometry for adeno-associated virus capsid titer measurement and applications to upstream and downstream process development

Thomas M. Leibiger,[1] Luke A. Remmler,[1] Erica A. Green,[1] and Kelvin H. Lee[1]

[1]University of Delaware, Department of Chemical and Biomolecular Engineering, Newark, DE, USA

Faster and more accurate analytical methods are needed to support the advancement of recombinant adeno-associated virus (rAAV) production systems. Recently, biolayer interferometry (BLI) has been developed for high-throughput AAV capsid titer measurement by functionalizing the AAVX ligand onto biosensor probes (AAVX-BLI). In this work, an AAVX-BLI method was evaluated using Octet AAVX biosensors across four rAAV serotypes (rAAV2, -5, -8, and -9) and applied in an upstream and downstream processing context. AAVX-BLI measured the capsid titer across a wide concentration range (1×10^{10}–1×10^{12} capsids/mL) for different rAAV serotypes and sample backgrounds with reduced measurement variance and error compared to an enzyme-linked immunosorbent assay (ELISA) method. Biosensors were regenerated for repeated use, with lysate samples showing reduced regeneration capacity compared to purified and supernatant samples. The AAVX-BLI method was applied in a transfection optimization study where direct capsid titer measurement of culture supernatants generated a representative response surface for the total vector genome (VG) titer. For rAAV purification, AAVX-BLI was used to measure dynamic binding capacity with POROS CaptureSelect AAVX affinity chromatography, showing resin breakthrough dependence on the operating flow rate. Measurement accuracy, serotype and sample background flexibility, and high sample throughput make AAVX-BLI an attractive alternative to other capsid titer measurement techniques.

INTRODUCTION

Recombinant viruses are used as gene therapy vectors because of their efficiency in delivering genetic material to cells *in vivo*.[1] Adeno-associated virus (AAV) has been widely used as a viral vector for *in vivo* gene therapies due to its ability to achieve long-lasting transgene expression in multiple tissue types while maintaining good safety and tolerance profiles.[2] At least 13 naturally occurring AAV serotypes have been identified, and additional serotypes have been engineered with rational design approaches.[3,4] Currently, there are 6 approved recombinant AAV (rAAV) gene therapies globally and over 200 completed or ongoing clinical trials involving rAAV gene therapies for the treatment of monogenic diseases.[5] Despite significant clinical success, low manufacturing capacities for rAAV products remain a barrier to widespread therapeutic availability.[6] Central to the development and characterization of improved manufacturing platforms is the establishment of analytical techniques for measuring critical quality attributes, such as the vector genome (VG) and capsid titer, full-to-empty capsid ratio, product purity, and other product- and process-related attributes.[7,8] These analytical methods are crucial for supporting design-of-experiment and other process development activities for transfection and cell culture process parameter optimization and downstream product purification.

Measurement of the capsid titer is typically performed using a serotype-specific enzyme-linked immunosorbent assay (ELISA), which is a labor-intensive process taking 2–5 h to complete with a typical variance ranging from 10% to 20%.[9] The commercial launch of the AAVX single-domain antibody fragment, which binds all naturally occurring and most synthetic AAV serotypes, has allowed for the development of new purification and analytical techniques.[10] Recently, the AAVX ligand has been applied for direct measurement of the AAV capsid titer by immobilization onto biolayer interferometry (BLI) biosensors. Label-free capsid concentration measurement is achieved by detection of white light interference patterns resulting from changes in the binding layer thickness at the tip of the biosensor.[11] In this work, we assessed the performance of AAVX-BLI using Octet AAVX biosensors for measurement of the capsid titer across four rAAV serotypes (rAAV2, -5, -8, and -9) and explored how this technique can be applied in a cell culture and purification context. Using internally produced rAAV reference material, we first tested the ability of AAVX-BLI to measure different rAAV serotypes across a wide range of concentrations (5.0×10^{9}–1.0×10^{12} capsids/mL) for purified and crude samples. We then compared AAVX-BLI to an ELISA method for capsid titer measurement, showing that AAVX-BLI measures samples across a wider range of concentrations with reduced variance, error, and active lab time. We demonstrated that multiplate AAVX-BLI biosensor regeneration is possible and biosensor regeneration capacity is primarily dependent on the sample

Received 28 February 2024; accepted 23 July 2024;
https://doi.org/10.1016/j.omtm.2024.101306.

Correspondence: Kelvin H. Lee, University of Delaware, Department of Chemical and Biomolecular Engineering, Newark, DE, USA.
E-mail: khl@udel.edu

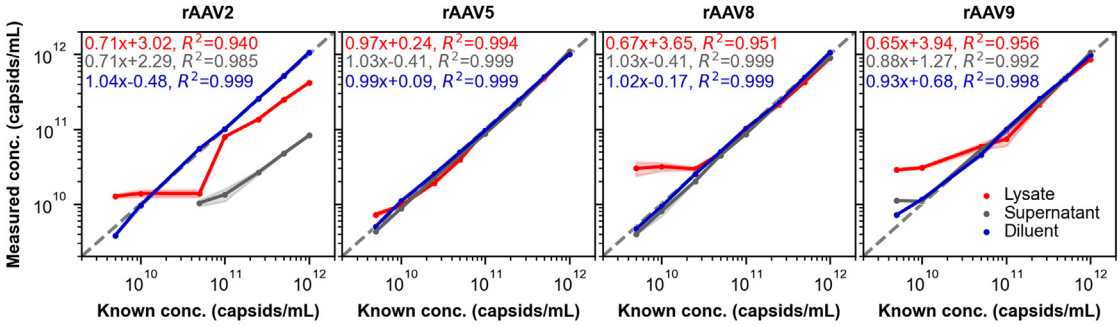

Figure 1. Capsid titer measurements using Octet AAVX with lysate, supernatant, and Octet Sample Diluent backgrounds

Octet AAVX-measured capsid titers for rAAV2, -5, -8, and -9 samples diluted in control lysate (red), control supernatant (gray), and Octet Sample Diluent (blue) plotted against the known concentration. The dashed gray lines indicate a line with a slope of m = 1, where measured and known concentrations would be equal. Equations for lines of best fit in $\log_{10}$ space and the goodness of fit, R^2, are shown in the top left corner of each subplot. Error banding corresponds to the standard deviation of duplicate concentration measurements. Sample readings for AAV2 at 5.00×10^9 and 1.00×10^{10} diluted in supernatant are not shown because they did not generate a signal.

matrix. We determined that the capsid titer can be used as a rapid readout in transfection optimization studies aiming to maximize the VG titer, allowing for significantly decreased analysis time and increased sample throughput. AAVX-BLI was then used to generate dynamic binding capacity (DBC) breakthrough curves of POROS CaptureSelect AAVX affinity resin, showing that DBC is dependent on both AAV serotype and operating flow rate. AAVX-BLI is an important new tool in the AAV analytics toolbox, offering serotype and sample background flexibility, low measurement variance across a wide capsid concentration range, and direct quantitation for high-throughput capsid titer measurement.

RESULTS

Octet AAVX measurement with different sample backgrounds

Measurements of rAAV2, -5, -8, and -9 diluted in human embryonic kidney 293 (HEK293) control lysate, control supernatant, and Octet Sample Diluent at 5.0×10^9–1.0×10^{12} capsids/mL were taken to explore the dynamic range with different sample backgrounds. Samples measured for all serotypes show agreement between known and measured sample concentrations in the Octet Sample Diluent matrix, as indicated by the slopes of the best-fit lines being close to 1, which corresponds to a perfect alignment between the known and measured concentrations (Figure 1). Of the four serotypes tested, rAAV2 and rAAV9 measurements deviated slightly from the known concentration only at 5×10^9 capsids/mL. Results for samples diluted in control supernatant were mixed. rAAV5 and rAAV8 were unaffected by the supernatant matrix, with the slope being close to 1 for the best-fit lines. rAAV9 measurements showed that the supernatant background matrix has an impact at 5×10^9 capsids/mL. rAAV2 measurements were suppressed across the whole measured concentration range in the supernatant matrix, and the low best-fit slope (m = 0.71) and high y-intercept (b = 2.29) show deviations from the expected measurements. Background interference was observed for samples measured in the control lysate within the range of 1.0×10^{10}–2.5×10^{10} capsids/mL, indicated by a serotype-specific flattening of measured concentrations in this testing range (Figure 1). Less lysate background interference was observed for rAAV5 (m = 0.97) samples compared to rAAV8 (m = 0.67) and rAAV9 (m = 0.65). Measurements of rAAV2 were again significantly impacted by the sample matrix across the entire tested concentration range, as indicated by the low best-fit slope (m = 0.71) and high y-intercept (b = 3.02).

Octet AAVX biosensor regeneration capacity

To evaluate the regeneration lifetime of the AAVX-BLI probes in different matrices, biosensor binding response loss was tracked across different rAAV8 capsid concentrations and sample backgrounds over four sample plates. Biosensor binding response loss was primarily dependent on the sample background matrix, with slight impacts of capsid concentration observed over 27 regeneration cycles (Figure 2A). For purified samples diluted in Octet Sample Diluent, biosensors retained greater than 85% of the initial binding response (nm/s) across all sample reads, with the highest sample concentration (1.0×10^{12} capsids/mL) showing the greatest binding response retention at 92.6% ± 2.0%. Samples diluted in control supernatant had similar probe regeneration capacity to purified samples diluted in Octet Sample Diluent, retaining greater than 83% of the initial binding response (nm/s) across all sample reads. For samples measured in both Octet Sample Diluent and control supernatant backgrounds, probe binding response loss appeared to be gradual across the regeneration cycle range evaluated. Notable binding response loss was seen for samples diluted in control lysate background. The normalized binding responses for samples diluted in the control lysate after the final regeneration cycle measured at 0%, 6.1% ± 0.5%, and 27.6% ± 2.8% for 1.0×10^{11}, 5.0×10^{11}, and 1.0×10^{12} capsids/mL, respectively. After observing poor regeneration capacity for measurements in the control lysate background, an extended regeneration protocol was tested to determine if probe regeneration was dependent on the number of regeneration cycles or contact time with the low-pH regeneration buffer. Increasing the regeneration cycle number and cycle time between sample reads and decreasing the sample read time for the measurement of samples in the control lysate corresponded with improved binding response retention across regeneration cycles (Figure 2B). The extended regeneration protocol resulted in normalized binding responses for lysate samples after the final regeneration

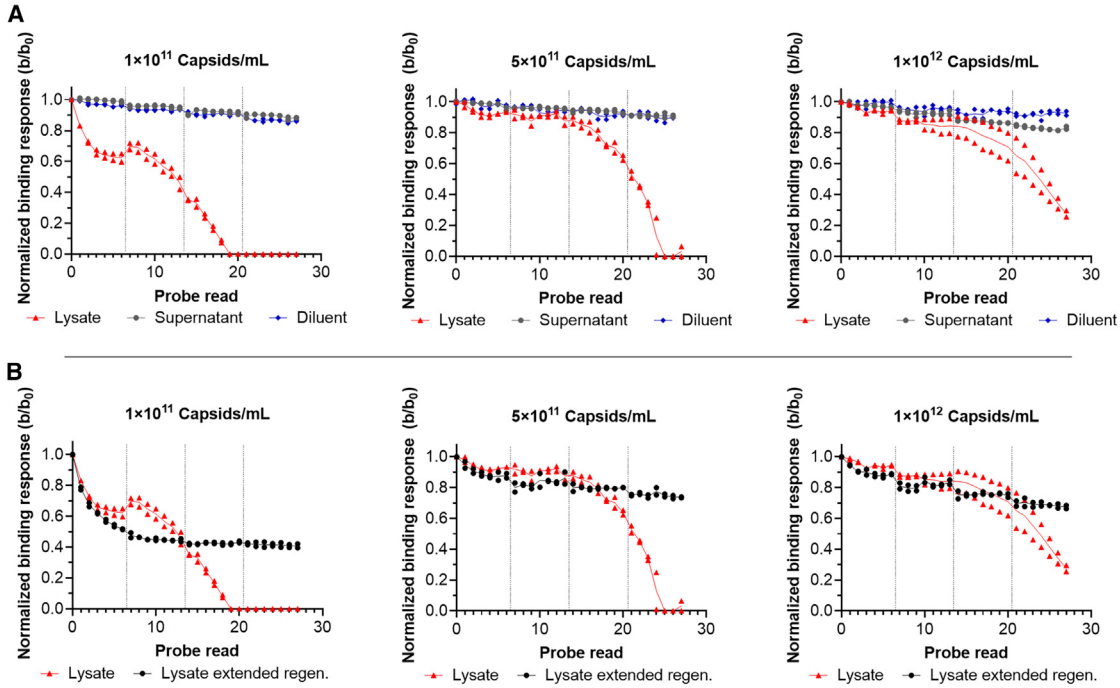

Figure 2. Octet AAVX biosensor regeneration capacity in lysate, supernatant, and Octet Sample Diluent backgrounds

(A) Octet AAVX biosensor normalized binding response (b/b_0) across 27 regeneration cycles for rAAV8 samples measured in control lysate (red triangles), control supernatant (gray dots), and Octet Sample Diluent (blue squares). (B) An extended regeneration protocol was applied for measurement of samples in control lysate background (black dots). Points are individual probe readings ($n = 2$), and lines represent the mean normalized binding response (b/b_0) at each read. Vertical gray dashed lines show where new sample plates were started. Data collected for measurements in control lysate with the initial regeneration protocol (red triangles) are plotted in both (A) and (B) for comparison.

cycle of 40.9% ± 1.9%, 73.7% ± 0.5%, and 67.5% ± 1.5% for 1.0×10^{11}, 5.0×10^{11}, and 1.0×10^{12}, respectively. For both regeneration methods, the normalized binding response decreased the most for the lowest sample concentration (1.0×10^{11} capsids/mL).

Orthogonal method comparison: ELISA vs. Octet AAVX capsid titer quantitation

Capsid titers measured using serotype-specific ELISA kits were compared to those measured by Octet AAVX biosensors to test the variability and limits of detection of the orthogonal methods. The slopes of the best-fit lines for all Octet AAVX and ELISA measurements for rAAV2 and rAAV5 were close to 1, indicating good agreement with the known concentrations (Figure 3A). Serotype-specific lower limits of detection for ELISA were observed for rAAV8 and rAAV9, as evidenced by the best-fit line slopes being less than 1 ($m_{AAV8} = 0.75$ and $m_{AAV9} = 0.89$, respectively) and y-intercepts being above 0 ($b_{AAV8} = 2.93$ and $b_{AAV9} = 1.41$). The relative standard deviation (RSD) for ELISA measurements was within the range of 5%–25%, compared to approximately 2% or less for the Octet AAVX method across all sample concentrations (Figure 3B). Measurements performed with the ELISA kits showed a 1-log range of capsid concentration, for which the error was below 10% (1.0×10^{11}–1.0×10^{12} capsids/mL pre-dilution), with error increasing when measuring samples outside of this range (Figure 3C). Comparatively, the Octet AAVX method yielded a measurement error of 5% or less across the 2-log concentration range tested (Figure 3C).

Upstream process application: Transfection optimization for VG and capsid titer

Across the design space tested, there was a trend of an increased VG titer with increased DNA mass delivery and DNA:FectoVIR-AAV ratio for both rAAV5 and rAAV8 (Figure 4A). This trend matched closely with the total capsid titer data generated using the Octet AAVX method, suggesting that the relative capsid titer is a reliable indicator of the relative VG titer for this system (Figure 4B). A representative surface response curvature was also generated from capsid titer data measured only from the culture supernatants (Figure 4C). This observation indicates that the capsid titer measured in the supernatant only can also be used as a surrogate for the total VG titer.

Analyzing VG and capsid titer data yielded similar outputs for variable significance and standardized effects of the two input variables on the response variable (Figure S1). The DNA:FectoVIR-AAV ratio had the strongest effect on VG, capsid, and supernatant capsid titers for both serotypes evaluated. The two-way variable interaction between DNA mass and DNA:FectoVIR-AAV ratio had statistically significant effects on all measured titers for both serotypes (Figure S1). Relationships between the input transfection parameters, output titers, and additional cell culture parameters were also explored (Figure 5). Increased DNA

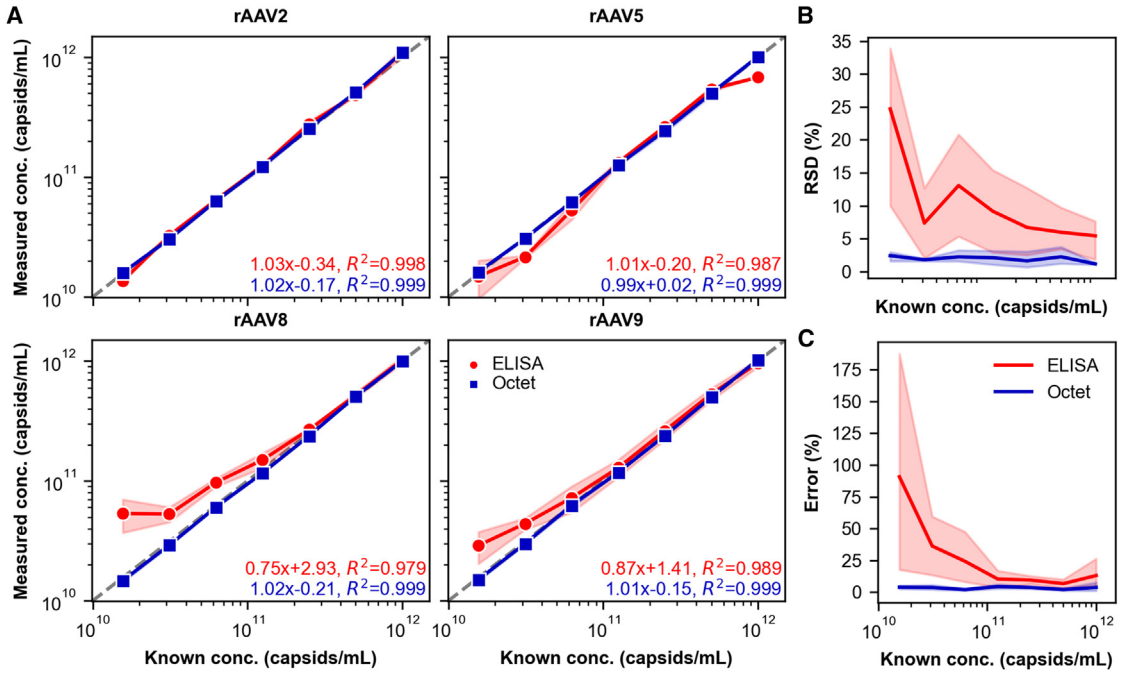

Figure 3. Capsid concentration measurements using ELISA and AAVX Octet

(A) Measured capsid concentrations using serotype-specific ELISA kits (red dots) and Octet AAVX BLI (blue squares) plotted against known concentrations with error banding corresponding to standard deviation (n = 3). The dashed gray lines indicate a line with a slope of m = 1, where measured and known concentrations would be equal. Equations for lines of best fit in $\log_{10}$ space and the goodness of fit, R^2, are shown in the top left corner of each subplot. (B) Relative standard deviation (RSD) and (C) error relative to the known concentration were calculated in aggregate across all four serotypes and all technical triplicates for each method. Error banding in (B) and (C) represent standard deviation of average concentration measurements (n = 3 technical replicates) of all rAAV serotypes (n = 4).

mass delivery corresponded with reduced culture viability and viable cell density at 72 h post-transfection for both serotypes. An increased capsid titer also corresponded with lower culture viability. A higher percentage of cells expressing enhanced green fluorescent protein (EGFP) at 24 h post-transfection corresponded with increased capsid and VG titers, and both titer values were positively correlated.

Downstream process application: DBC of POROS CaptureSelect AAVX resin

rAAV5 and rAAV8 breakthrough curves were generated to determine POROS CaptureSelect AAVX affinity chromatography DBC at different flow rates (Figure 6). The breakthrough curves show a higher DBC at 3 min residence time (RT) vs. 1 min RT for both serotypes. For rAAV5, the DBC at 5% breakthrough was 3.6×10^{14} capsids/mL resin at 1 min RT compared to 7.6×10^{14} capsids/mL resin at 3 min RT. For rAAV8, the DBC at 5% breakthrough measured 6.8×10^{14} capsids/mL resin at 1 min RT and 8.5×10^{14} capsids/mL resin at 3 min RT. Chromatograms showing ultraviolet (UV) absorbance at 280 nm vs. load volume and where individual load flowthrough fractions were collected during the process are shown in Figure S2.

DISCUSSION

The Octet AAVX method can measure a wide range of AAV capsid concentrations, although the measurement range differed depending on serotype and sample background. rAAV5 samples measured closely to the known concentrations in all three sample backgrounds down to 1.0×10^{10} capsids/mL, as indicated by regression line slopes for diluent, control supernatant, and control lysate backgrounds of 0.99, 1.03, and 0.97, respectively. rAAV8 and rAAV9 showed background interference preventing measurement below approximately 2.5×10^{10} capsids/mL in the control lysate background. Interestingly, rAAV5 showed a more rapid binding layer thickness accumulation compared to the other serotypes at the same capsid concentration, indicating a higher binding affinity for the AAVX ligand (Figures S3 and S4). This observation may be attributed to the AAV5 capsid structure, which is the most divergent AAV serotype, sharing less than 75% viral protein sequence homology with all other naturally occurring serotypes.[12–14] Binding characterization for AAV-specific affinity ligands has demonstrated serotype-specific divergence in binding epitopes.[15,16] Although rigorous binding epitope characterization of different AAV serotypes with the AAVX ligand has not been explored, Thermo Fisher Scientific has reported epitope mapping using cryo-transmission electron microscopy (cryo-TEM), which shows the capsid 5-fold axis binding to AAVX and unique AAV-AAVX contact residues for serotypes 2, 5, 8, and 9.[17] Variability in contact residues may impact capsid binding affinity or the steric orientation of bound capsids, leading to differences in binding layer accumulation in a BLI context. The

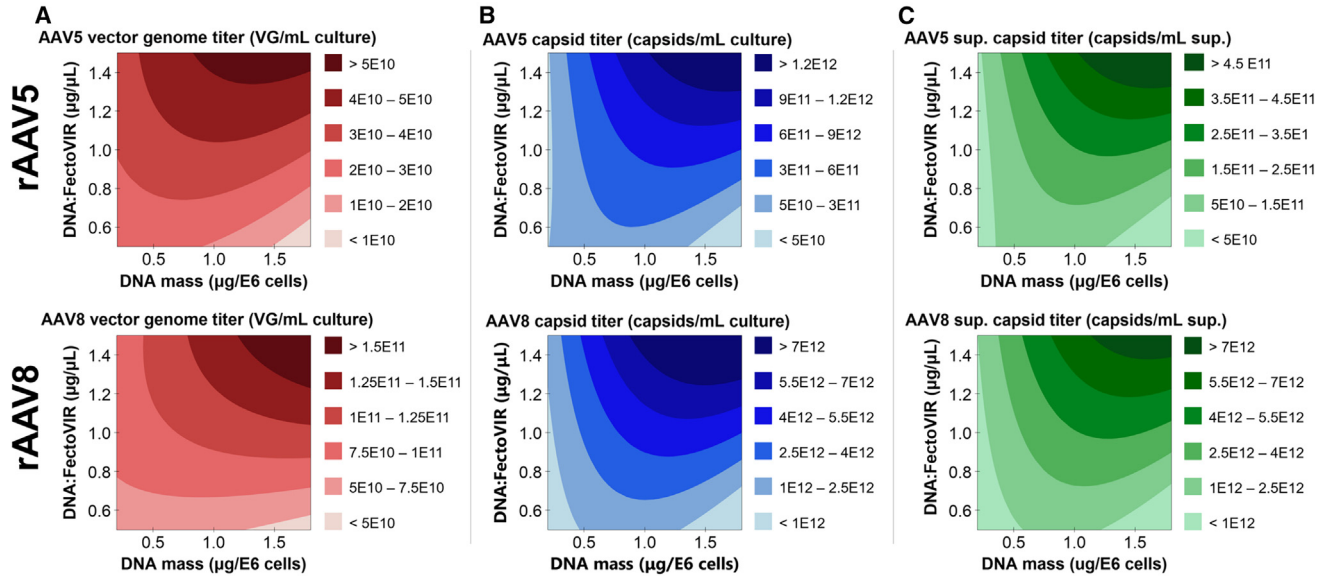

Figure 4. 2-factor surface response plots of total VG, total capsid, and supernatant capsid titers

rAAV5 (top row) and rAAV8 (bottom row) 2-factor surface response plots for VG (A, red), capsid (B, blue), and supernatant capsid (C, green) titers. Each titer was individually analyzed as a separate response variable using Minitab statistical software.

background interference observed when measuring rAAV8 and rAAV9 samples in control lysate is likely due to non-specific binding of host cell proteins (HCPs) to the AAVX ligand, which contributes to binding layer thickness accumulation. This effect is also observed when measuring rAAV9 in control supernatant below 1.0×10^{10} capsids/mL. rAAV9 displayed the most sensitivity to sample background interference at lower concentrations, which may be caused by a weaker binding affinity for the AAVX ligand, indicated by the slowest binding layer thickness accumulation of the serotypes evaluated (Figures S3 and S4). rAAV2 measurements trended differently when diluted in control lysate and control supernatant backgrounds compared to the other serotypes tested, with measured values reading lower than known concentrations. This trend may be attributed to the unique properties of AAV2, which, in comparison to AAV5, -8, and -9, is not highly secreted from HEK293 host cells during production and is known to have high affinity for heparin sulfate.[18,19] The presence of cell lysate and supernatant components may disrupt AAV2-AAVX ligand interactions through competitive binding or by promoting capsid aggregation. Overall, serotype-specific ranges of detection appear to be dependent on the binding kinetics of the serotype being analyzed and how they may be impacted by matrix components. While not assessed here, the transgene sequence and empty capsid percentage of an rAAV preparation may also alter the binding kinetics with AAVX. For these types of investigations, use of a reference standard that is representative of the test material by serotype, transgene, and approximate empty capsid percentage would be needed.

Biosensor regeneration capacity is an essential feature that impacts ease of use and cost of the AAVX-BLI method vs. orthogonal approaches. Results show that Octet AAVX biosensor regeneration capacity is primarily dependent on the sample matrix, with additional impacts from the AAV capsid concentration. Gradual binding response loss for measurements in Octet Sample Diluent and control supernatant backgrounds was observed along with slight increases to binding layer thickness accumulation during the baseline step, indicating carryover and re-binding of impurities (Figure S5). Binding response loss for samples measured in control lysate corresponded with the higher retention of bound matrix components through the regeneration process, as indicated by the increasing baseline height across extended sample reads (Figure S5). Decreased binding response loss across regeneration cycles with increased capsid concentration in the control supernatant background was observed. This decreased binding response loss may be due to a shielding effect of AAV capsid binding compared to background impurities, whereby capsids more readily dissociate from the biosensor surface than HCPs, but further testing is required to confirm this mechanism. Biosensor accumulation of bound matrix components is reduced for repeated measurements of samples diluted in control lysate with an extended regeneration protocol (Figure S5). Further reduction in binding response loss is likely possible but would require additional optimization of the regeneration process, examining parameters such as the number of regeneration cycles, the regeneration time, and the regeneration buffer pH and composition. Careful planning of plate maps for measurements where binding response loss is consistent and predictable can be used to mitigate the effects on matrix component accumulation. For instance, reference standards matching the test samples can be analyzed in parallel and used in the data analysis to correct for reduced biosensor binding response.

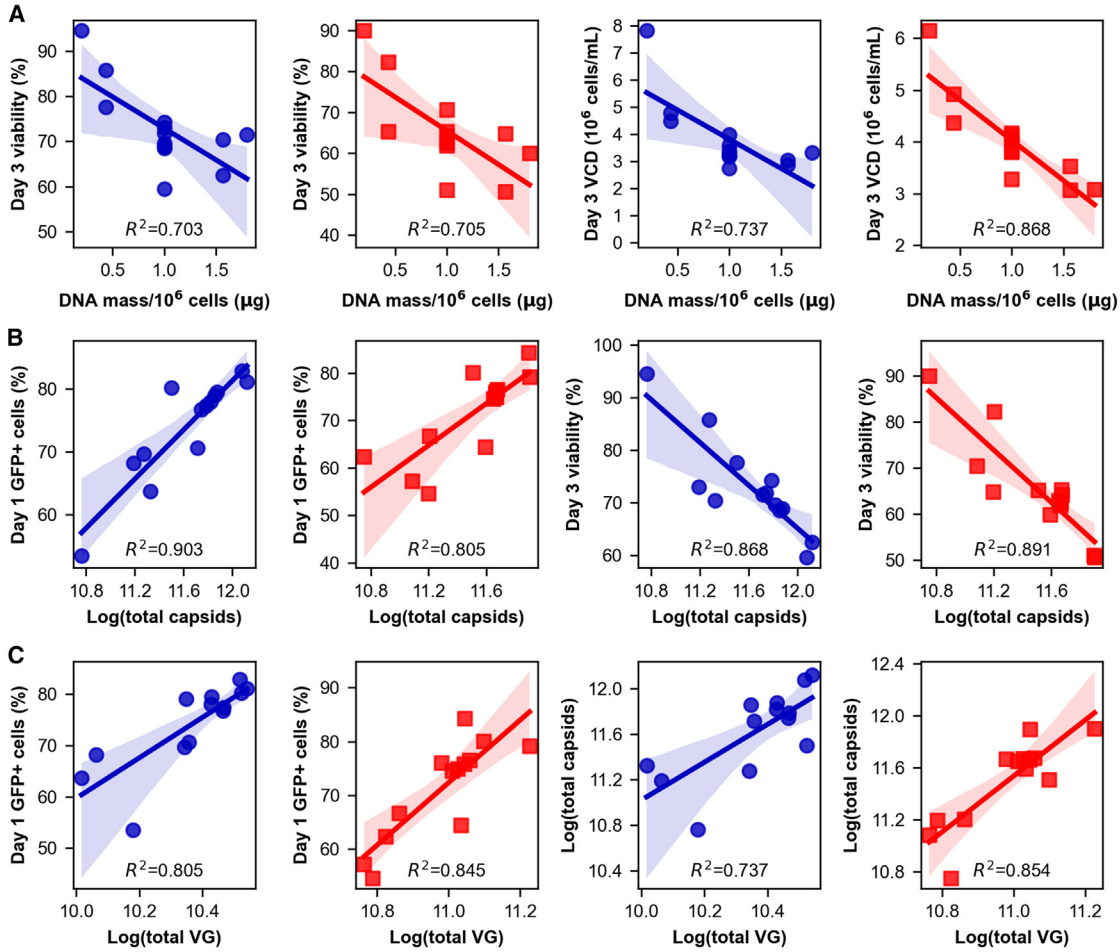

Figure 5. Regression plots of first-order relationships between transfection parameters and output titers

Regression plots showing first-order relationships with an input transfection parameter or an output titer for (A) DNA mass/10^6 cells, (B) the $\log_{10}$ of total capsids/mL, and (C) the $\log_{10}$ of total VG/mL. The points and regression lines are blue dots for rAAV5 and red squares for rAAV8. The colored banding indicates the 95% confidence interval.

Our ELISA data align with previously reported ranges for the RSD of AAV capsid sandwich ELISAs of 10%–20% and a linear measurement range of 1–2 orders of magnitude.[9] Compared to the ELISA method for capsid titer measurement, the Octet AAVX method was able to measure samples across a wider concentration range with reduced RSD and error. Based on the results, the Octet AAVX method can likely be applied beyond the 2-log concentration range examined. The reduced error and RSD for the Octet AAVX method can be attributed to direct quantitation of the AAV capsid titer, compared to the ELISA method, which requires multiple steps with the addition of a sample, a secondary antibody, a streptavidin peroxidase conjugate, and a tetramethylbenzidine substrate. The Octet AAVX method poses further benefits, as it required less than half the active lab time to generate data (20 vs. 55 min) despite taking a slightly longer total time (150 vs. 135 min) to run 16 samples in triplicate. Substitution of the ELISA capsid titer method with the Octet AAVX method can also allow for an improved estimation of the full-to-empty capsid ratio when combining capsid titer data with a VG titer method due to the Octet AAVX method's precision. While techniques such as analytical ultracentrifugation (AUC) or transmission electron microscopy (TEM) can directly measure the full-to-empty capsid ratio, making estimations with separate VG and capsid titer measurements is attractive because it avoids the throughput limitations and instrument requirements associated with TEM and AUC.

Transient rAAV production depends on the delivery of plasmids encoding essential viral capsid proteins (VP1, VP2, VP3), replication proteins (Rep40, Rep52, Rep68, Rep78), helper virus elements, and a gene of interest flanked by inverted terminal repeat regions. Due to host cell cytotoxicity resulting from viral protein expression and possible cytotoxic effects from transfection reagents, balancing the delivery of these elements is important for maximizing rAAV production and packaging. Transfection optimization studies are crucial for maximizing the dose-determining rAAV VG titer for transient production systems, but performing the titer measurements can be labor and time intensive.[20–23] Measuring the VG titer requires one or more treatments to

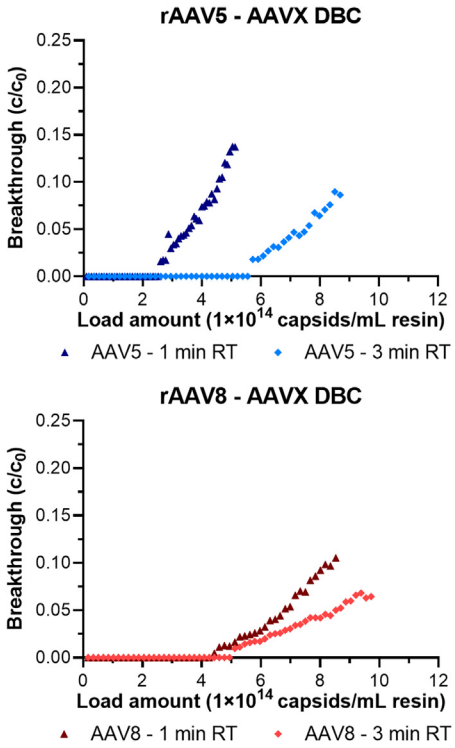

Figure 6. Load breakthrough curves for POROS CaptureSelect AAVX affinity chromatography

POROS CaptureSelect AAVX affinity chromatography load breakthrough curves for rAAV5 (left) and rAAV8 (right) at 1 and 3 min RT. Each point represents capsids loaded per mL resin calculated based on mean Octet AAVX measurements ($n = 2$).

remove exogenous DNA, digest capsids, and quantify released VGs using a digital droplet PCR or quantitative real-time PCR (real-time qPCR) method with transgene-specific primers and probe.[24] Each step requires manual sample manipulation, which can introduce errors and take multiple days to perform depending on the number of culture conditions. Our 2-factor surface response study results show that the total VG titer measured with real-time qPCR and the capsid titer measured with the Octet AAVX method analyzed as separate output variables give consistent standardized effect trends for statistically significant transfection parameters (Figures 4 and S1). The trending of the capsid titer with the VG titer has been observed previously, where, for instance, Coplan et al. reported data for multivariate rAAV production studies showing the correlation of VG and capsid titers as output variables, with high VG titer conditions corresponding with a high capsid titer.[22] Additionally, contour plots and standardized effect trends for capsid titer measurements of culture supernatants show conserved response curvature and statistically significant factors compared to total capsid and VG titers, indicating that culture performance for our system can be screened directly from samples following cell removal with no further treatment. Using the capsid titer as a surrogate for the expected VG titer can be applied across large screening studies examining multiple transfection parameters simultaneously, whereby a subset of conditions can be further evaluated for the VG titer using a PCR-based approach. This screening strategy can eliminate sample treatment steps, save time, and increase the number of experimental conditions that can be tested.

The 2-factor surface response study performed in this work was intended to demonstrate the ability of the Octet AAVX method to provide a rapid and high-throughput readout of the capsid titer in an upstream processing context. Response curvatures and optimal transfection conditions for rAAV production can vary widely by culture system and due to additional process variables, such as plasmid constructs, plasmid ratio, transfection reagent, and complexation protocol. More extensive explorations of transfection parameter design spaces have been performed for maximizing rAAV production.[22,23] Consistent with our findings, a previously published multivariate study examining transfection parameters for rAAV production identified the ratio of DNA:FectoVIR-AAV as having the largest single-variable effect on VG and capsid titers out of the factors examined.[22] Interestingly, this study also observed that applying the optimized transfection process for rAAV8 to the production of different rAAV serotypes showed statistically significant improvements in the VG titer, which aligns with our finding of consistent response curvatures for both rAAV5 and rAAV8.

The use of transient fluorescent protein expression as a proxy for the transfection efficiency of rAAV production genes can also simplify the analysis of screening studies using model vectors expressing fluorescent proteins. More efficient transport of plasmid DNA complexes to cells results in increased viral protein expression, which also corresponds with higher EGFP expression. In our system, the percentage of EGFP+ cells 24 h post-transfection was correlated with increased total capsid and VG titers. However, the balancing of increased delivery of viral elements with host cell cytotoxicity can be seen with a trend of decreased culture viability at 72 h post-transfection with higher DNA mass delivery (Figure 5C).

As rAAV production systems continue to shift toward scalable suspension culture formats with increasing titers, downstream processes have adapted with volume-reducing filtration steps and more scalable column chromatography methods for product capture and polishing.[10,25] Affinity column chromatography has emerged as a scalable and robust method for primary capture of rAAV capsids.[10] This method indiscriminately isolates capsids regardless of packaging, which allows process development to be performed through the assessment of capsid load and recovery. We generated POROS CaptureSelect AAVX affinity chromatography capsid breakthrough curves for rAAV5 and rAAV8 with 2% load volume resolution using the Octet AAVX method. The flow rate impacted DBC for both serotypes, with earlier and steeper breakthrough occurring at 1 compared to 3 min RT (Figure 6). The flow rate impacts were more apparent for rAAV5 under the conditions evaluated. This method for capsid titer can be applied to other downstream unit operations, such as anion-exchange chromatography, where tracking capsid removal along

with VG retention is desired. Due to the number of samples, trend sensitivity, and requirement of measuring crude samples, producing these data with other established capsid titer methods would be challenging.

MATERIALS AND METHODS

Reference material generation: rAAV production

EXPI293 cells (Thermo Fisher Scientific) were exchanged into fresh EXPI293 Expression Medium (Thermo Fisher Scientific) and seeded into 1 L shake flasks (Corning) at 2.5 × 10^6 viable cells/mL and 200 mL working volume. The following plasmids were purchased from Addgene: pAdDeltaF6 (pAdH, Addgene #112867), pAAV-GFP (pEGFP, Addgene #32395),[26] pAAV2/2 (pRep2/Cap2, Addgene #104963), pAAV2/5 (pRep2/Cap5, Addgene #104964), pAAV2/8 (pRep2/Cap8, Addgene #112864), and pAAV2/9n (pRep2/Cap9, Addgene #112865) (Table S1). For transfection of each 1 L flask, 1.57 μg total DNA/10^6 cells were diluted in Opti-Plex Complexation Buffer (Thermo Fisher Scientific) to 10 mL (5% culture volume) at a 1.5:1:1 (rAAV5, -8, and -9) or 5:1:0.31 molar plasmid ratio (rAAV2) of pRep2/CapX:pAdH:pEGFP. FectoVIR-AAV (Polyplus) transfection reagent was added to plasmid mixtures at a 1.35 μg DNA/μL FectoVIR-AAV ratio, followed by brief mixing and a 30 min complexation time. Complexed plasmid mixtures were added to cells dropwise while gently swirling the flasks, and the flasks were placed into a Multitron HT (Infors, 25 mm throw) incubator at 135 rpm, 37°C, 80% relative humidity (RH), and 5% CO_2 prior to being harvested at 72 h post-transfection. An additional 2 × 1 L flask of EXPI293 cells was transfected as described above but only included the pEGFP plasmid. These cultures were processed in parallel with the rAAV production cultures and used for the generation of control lysate and control supernatant materials. 0.5 mL culture samples were taken at 24, 48, and 72 h post-transfection for each culture and measured for culture viability using a Vi-Cell XR (Beckman Coulter) cell viability analyzer and for transient EGFP expression using an Accuri C6 Plus flow cytometer (BD) equipped for detection of EGFP (488 nm laser, 533/30 emission).

Reference material generation: Culture harvest, treatment, and real-time qPCR

Cells were pelleted by centrifuging at 1,000 RCF using a 5920 R benchtop centrifuge (Eppendorf) for 10 min. Supernatants were decanted and cell pellets were resuspended in 25 mL of Mammalian Lysis Buffer (50 mM TRIS-HCl, 150 mM NaCl, 2 mM $MgCl_2$ [pH 8.5]), followed by 3 freeze-thaw cycles. Lysate mixtures were treated with 25 U/mL Benzonase Nuclease (Sigma-Aldrich) for 60 min at 37°C. Cell debris was removed by centrifuging at 3,428 RCF using a 5920 R benchtop centrifuge (Eppendorf) followed by 0.2 μm vacuum filtration (Fisher Scientific). Supernatants were treated with 2 M $MgCl_2$ to a concentration of 2 mM and 25 U/mL Benzonase Nuclease (Sigma-Aldrich) for 60 min at 37°C followed by 0.2 μm vacuum filtration (Fisher Scientific). All supernatant and lysate samples were then treated with DNase I (New England Biolabs) for 60 min at 37°C (2.5 μL sample, 2.5 μL DNase I, 2.5 μL DNase buffer, 17.5 μL molecular biology water) and 2.5 μL of 20 mg/mL Proteinase K (Thermo Fisher Scientific) at 56°C for 90 min, followed by Proteinase K inactivation at 95°C for 30 min prior to real-time qPCR. Lysates and supernatants (samples) were measured separately for VG titer against a PvuII (New England Biolabs) linearized pEGFP plasmid standard curve diluted in molecular biology water (Figure S6). Linearized pEGFP plasmid was desalted with the QIAquick PCR Purification Kit (Qiagen), and the concentration was quantified by UV absorbance (A260) on a DS-11 FX+ (DeNovix) before serial dilution to generate a 7-point standard curve (10^9–10^3 copies per reaction). Samples were 10-fold diluted in molecular biology water after Proteinase K inactivation, and real-time qPCR was performed on a CFX384 Touch Real-Time PCR system (Bio Rad) using TaqMan Fast Advanced Master Mix (Thermo Fisher Scientific) and 900 nM primers/250 nM probe (IDT) targeting the EGFP transgene (Table S2). The VG titer was calculated on the basis of VG/mL culture individually for lysate and supernatant lots (Figure S7).

Reference material purification and capsid titer measurement

Lysate and supernatant material lots were combined pre-purification for rAAV5, -8, and -9, respectively, while rAAV2 was purified only from the lysate due to the low supernatant VG titer. Purifications were performed using a TRICORN 10/100 (Cytiva) column packed with 6 mL of fresh resin on an AKTA Avant (Cytiva) fast protein liquid chromatography system. Capto AVB (Cytiva) resin was used for rAAV2 and rAAV5, and POROS CaptureSelect AAVX (Thermo Fisher Scientific) resin was used for rAAV8 and rAAV9 purification. The following protocol was used: equilibration with 10 column volumes (CVs) of equilibration buffer (20 mM Tris-HCl, 0.5 M NaCl [pH 7.5]), product loading (lysate diluted 1:1 in equilibration buffer for rAAV2 or pooled lysate and supernatant for rAAV5, -8, and -9), washing with 15 CVs of equilibration buffer, and elution with 5 CVs of elution buffer (0.1 M glycine-HCl [pH 2.6]). Eluates were collected in 50 mL conical tubes (Fisher Scientific) containing 3 mL (10% v/v) 1 M Tris-HCl (pH 8.7) Neutralization Buffer. Chromatograms for reference material generation are shown in Figure S8. Neutralized elution pools were measured for the capsid titer on an Octet R8 (Sartorius) instrument as detailed below and quantified relative to reference vectors purchased from Addgene (Addgene 105530 for rAAV2, -5, -8, and -9) (Table S1). Internally produced, purified, and measured vector lots are referred to, respectively, as rAAV2, rAAV5, rAAV8, and rAAV9 or collectively as rAAV. HEK293 cultures transfected only with pEGFP were harvested into lysate and supernatant lots and processed in parallel with rAAV-producing HEK293 cultures through Benzonase Nuclease treatment and 0.2 μm vacuum filtration as described above. The lysate material was 3-fold diluted in 1× PBS to adjust for an increased cell density at harvest for the pEGFP-transfected cultures compared to the rAAV-producing cultures. Processed lysate (3-fold diluted) and supernatant from pEGFP-transfected HEK293 cultures are referred to as control lysate and control supernatant, respectively.

AAVX-BLI-Octet AAVX method and data analysis

Samples were analyzed with Octet AAVX biosensors (Sartorius) on an Octet R8 (Sartorius) instrument with the following method

parameters: 160 s buffer baseline step with Octet Sample Diluent (Sartorius), 600 s sample read step, 5 probe regeneration cycles, and 5 s probe regeneration cycle time with regeneration buffer (10 mM glycine-HCl [pH 1.7]). 200 μL of sample or buffer was loaded into black 96-well F-bottom microplates (Greiner) run at 30°C and 1,000 rpm shake speed. Probes were hydrated in Octet Sample Diluent for 5 min prior to a run, and fresh rAAV reference standards serially diluted in Octet Sample Diluent were used for each plate. Data analysis was performed using Octet Analysis Studio software v.12.2. "Dose Response – 4PL (Weighted Y)" was used to generate the standard curves. Curve fitting time windows were manually adjusted to cover the linear range of each sample binding curve as needed to obtain the most accurate fit for standards and samples. Binding curve saturation is concentration dependent, meaning that curve fitting time windows can be narrow (such as with the 5×10^{12} capsids/mL sample shown in Figure S3) or span the entire read time (such as with the 5×10^{10} capsids/mL sample shown in Figure S3).

AAVX Octet measurements with different sample backgrounds

rAAV2, -5, -8, and -9 vectors were serially diluted into three different sample backgrounds: Octet Sample Diluent, control lysate, and control supernatant. Each serotype was diluted to 1.00×10^{12}, 5.00×10^{11}, 2.50×10^{11}, 1.00×10^{11}, 5.00×10^{10}, and 1.00×10^{10} capsids/mL in each matrix and measured for the capsid titer using the Octet AAVX method. Samples were measured in duplicate, with each sample read performed using a separate AAVX biosensor.

AAVX biosensor regeneration capacity

Octet AAVX biosensor regeneration capacity was investigated for rAAV8 at three different capsid concentrations, 1.00×10^{12}, 5.00×10^{11}, and 1.00×10^{11} capsids/mL, and in three different sample backgrounds, Octet Sample Diluent, control lysate, and control supernatant. Each concentration and sample background pairing were measured in duplicate across 27 probe-regeneration cycles. To gauge the binding response loss vs. regeneration cycle number, the measured binding response (nm/s) at each sample read was normalized to the initial binding response at the first read, termed "b_0." To determine whether binding response loss is dependent on method parameters, an additional binding response study was performed for the control lysate sample matrix with the regeneration parameters adjusted to 10 cycles of 10 s with a 450 s sample read time. Doubling of the regeneration cycle number and contact time for the extended regeneration protocol was selected to allow for the increased exposure of probes to the low-pH regeneration buffer while avoiding excessive method runtime. The reduction of sample read time from 600 to 450 s was selected to give a reduced binding of background impurities while still allowing enough time for binding curves to sufficiently develop for each sample read. 1.00×10^{12}, 5.00×10^{11}, and 1.00×10^{11} capsid/mL samples of rAAV8 in control lysate were measured across 27 regeneration cycles using the extended regeneration protocol. All regeneration studies were performed in duplicate, with data across the 27 regeneration cycles collected using separate probes for each condition.

ELISA vs. Octet AAVX capsid titer quantitation

Test samples and reference standards were prepared by diluting the internally produced rAAV for each serotype in Octet Sample Diluent. Test samples were serially diluted to 1.00×10^{12}, 5.00×10^{11}, 2.50×10^{11}, 1.25×10^{11}, 6.25×10^{10}, 3.13×10^{10}, and 1.56×10^{10} capsids/mL. Reference standards were serially diluted to 1.20×10^{12}, 6.00×10^{11}, 3.00×10^{11}, 1.50×10^{11}, 7.50×10^{10}, 3.75×10^{10}, 1.88×10^{10}, and 9.38×10^{9} capsids/mL. Test samples were measured using the AAVX Octet method and quantified vs. a standard curve generated from the reference standards. ELISA was performed for the same test sample sets using AAV2, AAV5, AAV8, and AAV9 Xpress sandwich ELISA kits (Progen; PRAAV2XP, PRAAV5XP, PRAAV8XP, PRAAV9XP) following the manufacturer's protocol except for standard curve preparation, which used internally produced rAAV reference material to maintain alignment with the Octet AAVX method. Test samples and reference standards were further diluted using ELISA Assay Buffer (Progen) to be within the range of detection as specified by the kit protocols. Absorbance was measured between 450 and 470 nm using a SpectraMax M5 plate reader (Molecular Devices), and readings were corrected by subtracting the background absorbance read at 650 nm. Samples were run in triplicate for both methods to allow for higher-confidence comparisons between the methods. Triplicate sample reads for the Octet AAVX method were performed using three separate biosensors.

Transfection optimization for VG and capsid titer

Total DNA mass delivery (0.2–1.8 μg/10^6 cells) and DNA:FectoVIR-AAV ratio (0.5–1.5 μg DNA/μL FectoVIR-AAV) for transfection were explored using a full factorial 2-factor central composite response surface study (Table S3). 13 transfections were performed in duplicate for cultures producing rAAV5 and rAAV8. EXPI293 cells were exchanged into fresh EXPI293 Expression Medium and seeded into 50 mL TPP vented bioreactor tubes (Sigma-Aldrich) at a viable cell density of 2.5×10^6 cells/mL in a 7.5 mL culture volume. Plasmid DNA was complexed together for duplicate conditions—pRep2/Cap5 or pRep2/Cap8, pAdH, and pEGFP plasmid DNA corresponding to each test condition were diluted with Opti-Plex Complexation Buffer (Thermo Fisher Scientific) to a volume of 1 mL in 1.5 mL microcentrifuge tubes (VWR). FectoVIR-AAV (Polyplus) was added to each tube, tubes were vortexed briefly and incubated for 30 min, and 375 μL of complexation was added to each culture. Bioreactor tubes were placed into a Multitron HT (Infors, 25 mm throw) incubator at 200 rpm, 37°C, 80% RH, and 5% CO_2 prior to being harvested at 72 h post-transfection. 0.5 mL culture samples were taken at 24, 48, and 72 h post-transfection. Culture samples were measured for cell density and viability on a Vi-Cell XR cell viability analyzer (Beckman Coulter) and for EGFP expression using an Accuri C6 Plus flow cytometer (BD) equipped for detection of EGFP (488 nm laser, 533/30 emission). At harvest, each culture was separated into lysate and supernatant lots by centrifuging at 1,000 RCF using a 5920 R benchtop centrifuge (Eppendorf), decanting supernatants, and resuspending cell pellets in 2.5 mL Mammalian Lysis Buffer followed by Benzonase Nuclease (Sigma-Aldrich) and DNase I (New England Biolabs) treatment as previously described. VG titer measurement with

real-time qPCR and capsid titer measurement with Octet AAVX were performed for each lysate and supernatant lot as previously described. Capsid titers were measured in duplicate using two separate AAVX biosensors, and the average values for the duplicate reads were used for statistical analyses. The VG titer and capsid titer were analyzed as separate response variables vs. DNA mass and DNA:FectoVIR-AAV ratio using Minitab statistical software v.21.1 with a 95% confidence interval. An additional analysis was performed for the capsid titer measured only in sample supernatants.

DBC of POROS CaptureSelect AAVX affinity chromatography resin

DBC was evaluated for POROS CaptureSelect AAVX affinity chromatography resin using the Octet AAVX method for rAAV5 and rAAV8 at 1 and 3 min RT. An additional 2 × 1 L shake flask of rAAV5 and rAAV8 was produced and harvested as described previously. Lysates and supernatants for each serotype were pooled together after harvest treatment and measured for the capsid titer using Octet AAVX with rAAV5 and rAAV8 standard curves. Material pools were 0.2 μm vacuum filtered (Fisher Scientific) immediately prior to chromatography loading. For each run, 0.25 mL of fresh POROS CaptureSelect AAVX resin (Thermo Fisher Scientific) was packed in a TRICORN 5/50 column (Cytiva) equipped with two top adapters. Columns were equilibrated with 10 CVs of equilibration buffer followed by loading of pooled lysate and supernatant (25 mL for rAAV8 1 min RT, 25 mL for rAAV8 3 min RT, 25 mL for rAAV5 1 min RT, and 50 mL for rAAV5 3 min RT), with flowthrough fractions collected every 2% of the load block into 96-deep well plates (Greiner). Load flowthrough fractions were 10-fold diluted in Octet Sample Diluent and measured for the capsid titer in duplicate using Octet AAVX with rAAV5 and rAAV8 standard curves. Duplicate samples were read using separate biosensors. Capsid breakthrough was determined by plotting the average capsid concentration of each fraction divided by capsid concentration of the load material (c/c_0) vs. capsid load amount (capsids/mL resin). DBC at 5% breakthrough was determined by the calculated capsid load (capsids/mL resin) at the first point where c/c_0 exceeded 0.05.

Statistical analysis

Data were processed and figures generated using GraphPad (v.10.1.2), Python (v.3.9.17), or Minitab (v.21.1). A p value of <0.05 was considered significant for data processed in Minitab. Flow cytometry data analysis was performed using BD CSampler Plus Software v.1.0.27.1 and Python v.3.9.17 with FlowKit v.1.0.1.

DATA AND CODE AVAILABILITY

All data generated or analyzed during this study are included in this published article and its supplemental information files or are available upon reasonable request.

SUPPLEMENTAL INFORMATION

Supplemental information can be found online at https://doi.org/10.1016/j.omtm.2024.101306.

ACKNOWLEDGMENTS

The authors are grateful to Sartorius for providing Octet AAVX biosensors. This work was supported in part by financial assistance award 70NANB17H002 from the US Department of Commerce, National Institute of Standards and Technology. The graphical abstract figure was created with BioRender.com.

AUTHOR CONTRIBUTIONS

T.M.L., E.A.G., and K.H.L. conceptualized the research; T.M.L. designed the experiments; T.M.L. and L.A.R. performed the experiments; T.M.L. wrote the original draft; E.A.G., L.A.R., and K.H.L. edited the draft; and K.H.L. secured funding and provided supervision.

DECLARATION OF INTERESTS

Some of the consumables used in this research were provided by Sartorius, the manufacturer of the Octet system. Sartorius paid open access publication fees after manuscript acceptance. All experimental designs, analyses, and interpretations of data were performed by the authors independently.

REFERENCES

1. Goswami, R., Subramanian, G., Silayeva, L., Newkirk, I., Doctor, D., Chawla, K., Chattopadhyay, S., Chandra, D., Chilukuri, N., and Betapudi, V. (2019). Gene Therapy Leaves a Vicious Cycle. Front. Oncol. *9*, 297. https://doi.org/10.3389/fonc.2019.00297.

2. Clement, N., and Grieger, J.C. (2016). Manufacturing of recombinant adeno-associated viral vectors for clinical trials. Mol. Ther. Methods Clin. Dev. *3*, 7. https://doi.org/10.1038/mtm.2016.2.

3. Srivastava, A. (2016). In vivo tissue-tropism of adeno-associated viral vectors. Curr. Opin. Virol. *21*, 75–80. https://doi.org/10.1016/j.coviro.2016.08.003.

4. Wang, D., Tai, P.W.L., and Gao, G. (2019). Adeno-associated virus vector as a platform for gene therapy delivery. Nat. Rev. Drug Discov. *18*, 358–378. https://doi.org/10.1038/s41573-019-0012-9.

5. Clinicaltrials.gov (accessed November 8, 2023). https://clinicaltrials.gov/search?intr=AAV.

6. Fu, Q., Polanco, A., Lee, Y.S., and Yoon, S. (2023). Critical challenges and advances in recombinant adeno-associated virus (rAAV) biomanufacturing. Biotechnol. Bioeng. *120*, 2601–2621. https://doi.org/10.1002/bit.28412.

7. Wright, J.F. (2020). Quality Control Testing, Characterization and Critical Quality Attributes of Adeno-Associated Virus Vectors Used for Human Gene Therapy. Biotechnol. J. *16*, e2000022. https://doi.org/10.1002/biot.202000022.

8. Green, E.A., and Lee, K.H. (2021). Analytical methods to characterize recombinant adeno-associated virus vectors and the benefit of standardization and reference materials. Curr. Opin. Biotechnol. *71*, 65–76. https://doi.org/10.1016/j.copbio.2021.06.025.

9. Gimpel, A.L., Katsikis, G., Sha, S., Maloney, A.J., Hong, M.S., Nguyen, T.N.T., Wolfrum, J., Springs, S.L., Sinskey, A.J., Manalis, S.R., et al. (2021). Analytical methods for process and product characterization of recombinant adeno-associated virus-based gene therapies. Mol. Ther. Methods Clin. Dev. *20*, 740–754. https://doi.org/10.1016/j.omtm.2021.02.010.

10. Florea, M., Nicolaou, F., Pacouret, S., Zinn, E.M., Sanmiguel, J., Andres-Mateos, E., Unzu, C., Wagers, A.J., and Vandenberghe, L.H. (2023). High-efficiency purification of divergent AAV serotypes using AAVX affinity chromatography. Mol. Ther. Methods Clin. Dev. *28*, 146–159. https://doi.org/10.1016/j.omtm.2022.12.009.

11. Müller-Esparza, H., Osorio-Valeriano, M., Steube, N., Thanbichler, M., and Randau, L. (2020). Bio-Layer Interferometry Analysis of the Target Binding Activity of CRISPR-Cas Effector Complexes. Front. Mol. Biosci. *7*, 98. https://doi.org/10.3389/fmolb.2020.00098.

12. Van Vliet, K., Mohiuddin, Y., McClung, S., Blouin, V., Rolling, F., Moullier, P., Agbandje-McKenna, M., and Snyder, R.O. (2009). Adeno-associated virus capsid serotype identification: Analytical methods development and application. J. Virol. Methods *159*, 167–177. https://doi.org/10.1016/j.jviromet.2009.03.020.

13. Bantel-Schaal, U., Delius, H., Schmidt, R., and zur Hausen, H. (1999). Human adeno-associated virus type 5 is only distantly related to other known primate helper-dependent parvoviruses. J. Virol. *73*, 939–947. https://doi.org/10.1128/jvi.73.2.939-947.1999.

14. Mietzsch, M., Jose, A., Chipman, P., Bhattacharya, N., Daneshparvar, N., McKenna, R., and Agbandje-McKenna, M. (2021). Completion of the AAV Structural Atlas: Serotype Capsid Structures Reveals Clade-Specific Features. Viruses *13*, 101. https://doi.org/10.3390/v13010101.

15. Mietzsch, M., Smith, J.K., Yu, J.C., Banala, V., Emmanuel, S.N., Jose, A., Chipman, P., Bhattacharya, N., McKenna, R., and Agbandje-McKenna, M. (2020). Characterization of AAV-Specific Affinity Ligands: Consequences for Vector Purification and Development Strategies. Mol. Ther. Methods Clin. Dev. *19*, 362–373. https://doi.org/10.1016/j.omtm.2020.10.001.

16. Wang, Q., Lock, M., Prongay, A.J., Alvira, M.R., Petkov, B., and Wilson, J.M. (2015). Identification of an adeno-associated virus binding epitope for AVB sepharose affinity resin. Mol. Ther. Methods Clin. Dev. *2*, 15040. https://doi.org/10.1038/mtm.2015.40.

17. Drulyte, I., Raaijmakers, H., Hermans, P., Adams, H., and Radjainia, M. (2022). Cryo-EM structure of AAV8 and epitope mapping of CaptureSelect AAVX. Materials and Structural Analysis Division, *WP0030-EN-02-2022* (Thermo Fisher Scientific).

18. Vandenberghe, L.H., Xiao, R., Lock, M., Lin, J., Korn, M., and Wilson, J.M. (2010). Efficient Serotype-Dependent Release of Functional Vector into the Culture Medium During Adeno-Associated Virus Manufacturing. Hum. Gene Ther. *21*, 1251–1257. https://doi.org/10.1089/hum.2010.107.

19. Kern, A., Schmidt, K., Leder, C., Müller, O.J., Wobus, C.E., Bettinger, K., Von der Lieth, C.W., King, J.A., and Kleinschmidt, J.A. (2003). Identification of a heparin-binding motif on adeno-associated virus type 2 capsids. J. Virol. *77*, 11072–11081. https://doi.org/10.1128/jvi.77.20.11072-11081.2003.

20. Zhao, H., Lee, K.J., Daris, M., Lin, Y., Wolfe, T., Sheng, J., Plewa, C., Wang, S., and Meisen, W.H. (2020). Creation of a High-Yield AAV Vector Production Platform in Suspension Cells Using a Design-of-Experiment Approach. Mol. Ther. Methods Clin. Dev. *18*, 312–320. https://doi.org/10.1016/j.omtm.2020.06.004.

21. Meade, O., Clark, J., McCutchen, M., and Kerwin, J. (2021). Exploring the design space of AAV transient-transfection in suspension cell lines. Methods Enzymol. *660*, 341–360. https://doi.org/10.1016/bs.mie.2021.08.003.

22. Coplan, L., Zhang, Z., Ragone, N., Reeves, J., Rodriguez, A., Shevade, A., Bak, H., and Tustian, A.D. (2024). High-yield recombinant adeno-associated viral vector production by multivariate optimization of bioprocess and transfection conditions. Biotechnol. Prog. *40*, e3445. https://doi.org/10.1002/btpr.3445.

23. Fu, Q., Lee, Y.S., Green, E.A., Wang, Y., Park, S.Y., Polanco, A., Lee, K.H., Betenbaugh, M., McNally, D., and Yoon, S. (2023). Design space determination to optimize DNA complexation and full capsid formation in transient rAAV manufacturing. Biotechnol. Bioeng. *120*, 3148–3162. https://doi.org/10.1002/bit.28508.

24. Jiang, Z., and Dalby, P.A. (2023). Challenges in scaling up AAV-based gene therapy manufacturing. Trends Biotechnol. *41*, 1268–1281. https://doi.org/10.1016/j.tibtech.2023.04.002.

25. Kilgore, R., Minzoni, A., Shastry, S., Smith, W., Barbieri, E., Wu, Y., Lebarre, J.P., Chu, W., O'Brien, J., and Menegatti, S. (2023). The downstream bioprocess toolbox for therapeutic viral vectors. J. Chromatogr. A *1709*, 464337. https://doi.org/10.1016/j.chroma.2023.464337.

26. Gray, J.T., and Zolotukhin, S. (2011). Design and Construction of Functional AAV Vectors. Methods Mol. Biol. *807*, 25–46. https://doi.org/10.1007/978-1-61779-370-7_2.